

Experimental Investigation of Locomotion Efficiency and Path-Following for Underwater Snake Robots with and without a Caudal Fin[☆]

E. Kelasidi^{a,*}, A. M. Kohl^a, K. Y. Pettersen^a, B. H. Hoffmann^b, J. T. Gravdahl^b

^a*Centre for Autonomous Marine Operations and Systems, Dept. of Engineering Cybernetics at NTNU, NO-7491 Trondheim, Norway.*

^b*Dept. of Engineering Cybernetics at NTNU, NO-7491 Trondheim, Norway.*

Abstract

Over the last few decades, the robotics community has shown increasing interest in developing bioinspired swimming robots, driven by the need for more economical, more efficient, autonomous, highly flexible and maneuverable robotic systems for underwater operations. In this paper, we present a bioinspired underwater snake robot (USR) equipped with a passive caudal (tail) fin. In particular, a highly flexible USR configuration is presented that is capable of locomotion both on the ground and underwater due to its robust mechanical and modular design, which allows additional effectors to be attached to different modules of the robot depending on the requirements of the application. This provides flexibility to the operator, who can thus choose the proper configuration depending on the task to be performed in various uncertain environments on the ground and underwater. Experimental results on locomotion efficiency and path-following control are obtained for a physical USR to enable a comparison of the USR motion with and without the passive caudal fin, for both lateral undulation and eel-like motion patterns. Results comparing the locomotion efficiency in both simulations and experiments are presented in order to validate the proposed models for USRs. By means of fluid parameter identification, both a qualitative and a quantitative comparison between the simulated and experimental results are performed regarding the achieved forward velocity. Furthermore, the experimental results show that a path-following control approach that has previously been proposed for USRs without a caudal fin can be directly applied to solve the path-following control problem for this bioinspired USR with a passive caudal fin. In particular, it is shown that this path-following control approach successfully steers the robot toward and along the desired path, and furthermore, the results show that it is possible to almost double the forward velocity of the robot by using a passive caudal fin.

[☆]Research partly funded by VISTA, a basic research program in collaboration between The Norwegian Academy of Science and Letters and Statoil, and partly supported by the Research Council of Norway through its Centres of Excellence funding scheme, project no. 223254-NTNU AMOS.

*Corresponding author

Email address: eleni.kelasidi@ntnu.no (E. Kelasidi)

Keywords: Marine systems, Maritime robotics, Mechatronics, Intelligent autonomous vehicles, Underwater snake robot with a passive caudal (tail) fin, Locomotion, Efficiency, Line-of-sight (LOS) path-following control.

1. Introduction

Recently, there has been increasing interest in using bioinspired robotic systems as an alternative to the traditional remotely operated vehicles (ROVs) or autonomous underwater vehicles (AUVs) for underwater applications in the oil and gas industry, biology, marine archaeology, and other fields. In addition, many research groups studying bioinspired robots argue that it is essential to increase the agility and maneuverability of underwater robots. These features are essential for operations at subsea installations and in highly uncertain subsea environments [1, 2, 3, 4, 5, 6, 7, 8]. Hence, the robotics community is seeking new solutions suitable for the exploration, monitoring, surveillance and maintenance of subsea infrastructures. Swimming snake robots, which are bioinspired robotic systems that mimic the motion of biological snakes or eels, possess inherent manipulation capabilities and can thus be considered good candidates for these types of applications [8].

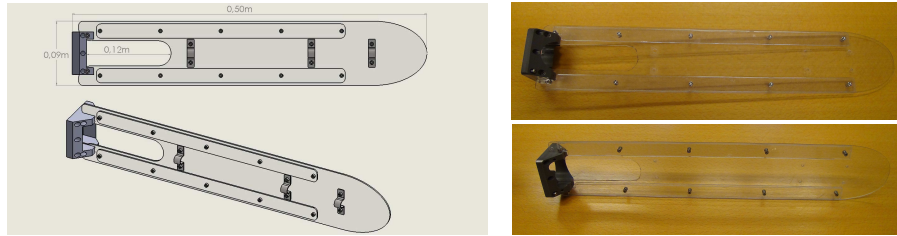
Several bioinspired swimming snake robots have been developed by different research groups [1, 2, 3, 4, 9, 10, 11, 12, 13, 14, 15, 16, 17]. Most of the swimming snake-like robots developed to date are modular multi-articulated robotic systems. However, when it comes to underwater snake robots with additional effectors (caudal fin, fins, thrusters), only a few physical systems have been implemented [3, 4, 18]. In [3, 4, 11, 17], the concept of using a caudal fin on the last segment, in addition to the joint-actuated motion of the USR, was presented. In particular, a new biorobotic platform inspired by the lamprey was developed as part of the Lampetra project [4]. In this concept, a multi-layer fiberglass tail is attached to the last segment of the robot to ensure good fluid dynamic behavior and propulsion of the robotic platform [4]. A lamprey-inspired robot was implemented based on biomimetic neurotechnology by [19]. This robot is functionally a three-component system consisting of a rigid hull/electronics bay, a flexible body axis supporting the Nitinol actuator, and a thin, passive caudal fin. Another swimming robot called AmphiBot III, presented in [3], consists of eight segments, with the first being the head segment and a caudal fin attached to the last segment (tail segment). A novel concept for an underwater swimming manipulator (USM) with additional thrusters was presented in [5, 6], and the first developed underwater snake robot to combine a bioinspired USR with a tail thruster module in the last segment was presented in [18]. However, the development of more efficient and robust configurations of underwater swimming robots by choosing the proper effectors to increase efficiency, with the overall goal of realizing operational snake robots for underwater applications, is still an open research area. Preliminary results for path-following of USRs with and without a caudal fin have been presented in [20]. However, in this paper we extend the results presented in [20] by obtaining comparison results for locomotion efficiency of USRs with and without caudal fin.

A new configuration of the underwater snake robot Mamba [8, 16] is presented, in which the joint-actuated links are combined with a passive caudal fin attached to the

last module of the robot. This is an interesting configuration because of two advantages compared with the configuration with thrusters [18]: it does not produce significant noise, and it will not perturb its surroundings as much as thrusters, which sometimes beat up silt from the seafloor, thereby decreasing visibility during operations in a sub-
45 sea environment. These features can be considered essential for various applications in underwater environments, including archaeological investigations of shipwrecks and underwater biological monitoring without disturbing the target creatures [7]. In this paper, we investigate whether a passive caudal fin offers advantages with respect to the achieved forward velocity compared with using only joint actuation for propulsion. We
50 present experimental results for two configurations of the robot, with and without a caudal fin, which show that compared with the configuration presented in [16, 8], attaching a passive caudal fin makes it possible to increase the forward velocity by almost 100%. In particular, the obtained results show that the average forward velocity for both lateral undulation and eel-like motion patterns is increased to almost double by using
55 the USR configuration with a passive caudal fin. Furthermore, results comparing the locomotion efficiency between simulations and experiments are presented to validate the models proposed for USRs. Specifically, in [21], the locomotion efficiency of USRs was studied by experimentally investigating fundamental properties of the velocity and power consumption of a USR without added effectors for both lateral undulation and
60 eel-like motion patterns. However, in [21], it was only possible to achieve a qualitative comparison and not a quantitative comparison between the simulated and experimental results. In this paper, by performing a precise experimental identification of the fluid parameters of Mamba, both a qualitative and a quantitative comparison between the simulated and experimental results are achieved with regard to the achieved forward
65 velocity.

Furthermore, to perform another comparative experimental study between physical robots with and without a passive caudal (tail) fin, we consider the case of path-following control. Specifically, we present experimental results for a USR with a passive caudal fin obtained using the path-following control approach previously proposed
70 and experimentally validated for underwater snake robots without a caudal fin in [8]. Preliminary results on path-following control were presented in [20]. The experimental results presented in this paper show that this path-following control approach can be directly applied to solve the path-following control problem for this bioinspired USR with a passive caudal fin. In particular, it is shown that this path-following control
75 approach successfully steers the robot toward and along the desired path, while it is simultaneously possible to nearly double the forward velocity.

This paper is organized as follows: Section 2 presents the configuration of the underwater snake robot Mamba with a passive caudal (tail) fin, and the modeling of USRs is outlined in Section 3. Experimental results for the locomotion efficiency and
80 path-following of Mamba that enable a comparison of its motion with and without a caudal fin are presented in Section 4. Finally, Section 5 presents the conclusions of this work, followed by suggestions for further research.



(a) Passive caudal (tail) fin.



(b) Underwater snake robot Mamba with a passive caudal fin attached to the last module of the robot.

Figure 1: Biologically inspired underwater snake robot with a caudal fin.

2. Underwater Snake Robot Mamba with and without a Passive Caudal Fin

Several bioinspired underwater snake-like robots (also referred to as eel-like robots) have been developed by different groups over the past few decades [1, 2, 3, 4, 9, 10, 11, 12, 13, 14, 15, 16, 17]. The underwater snake robot Mamba, which is presented briefly in this paper, was developed at NTNU in Norway. A more detailed description of the robot can be found in [8, 16]. The robot is capable of locomotion both on the ground and underwater due to its robust mechanical design, which allows additional effectors (e.g., caudal fin, pectoral fins, thrusters) to be attached to different modules of the robot depending on the requirements of the application. Hence, the robot has a highly flexible and reconfigurable nature that makes it attractive as a testbed for experimental investigations of various USRs with and without thrusters were presented. In this paper, we present a configuration in which the robot is equipped with a passive caudal fin attached to the last segment of the robot.

In this configuration, the underwater snake robot Mamba (see Fig. 1) consists of 18 modules that are watertight down to a depth of approximately 5 m, with a common mechanical and electrical interface between the modules, a head module and a passive caudal fin attached to the last module of the robot. A Hitec servo motor (HSR 5990TG) is used for the actuation of each of the 18 joint modules, and a microcontroller card (TITechSH2 Tiny Controller from HiBot) is used for the implementation of the necessary low-level control of each joint. In addition, each module contains a

force/torque sensor, temperature sensors, a 3-axis accelerometer and sensors for detecting water leakage. A CAN bus is used for communication among all microcontrollers in the modules of the robot, for sending the required reference signals to the robot and for reading the necessary data from the sensors installed inside the modules. Power supply cables (35 V) run through all the modules along with the CAN bus.

The caudal fin has a length of 0.5 m and a height of 0.09 m, identical to the height of the modules of the robot. The design of the caudal fin in SolidWorks and photographs of the developed caudal fin are shown in Fig. 1a. The strengtheners and holder of the caudal fin were made using polycarbonate (PC) and polyvinyl chloride (PVC), respectively. Note that an opening of 0.12 m on the caudal fin, close to the connection point, and additional attachment holders are required for the tether connection. In addition, during the experiments, the caudal fin was covered with a thin drysuit neoprene material to make it neutrally buoyant.

The modules of Mamba are mounted horizontally and vertically in an alternating fashion to provide locomotion capabilities in 3D space [16]. The robot consists of 20 links of length $2l = 0.18$ m and mass $m \approx 0.8$ kg. In this configuration, Mamba has a slightly positive buoyancy. In addition, the robot is covered with a watertight skin to provide an additional water barrier, as shown in Fig. 1b. Groundsheet, nylon, PU-coated, 120 g/m² material and rubber bottle wrist seals are used for the skin and the sealing of the head and tail parts, respectively. Note that during the experiments presented in Section 4, the angles of the joints responsible for the vertical motion were set to zero degrees to constrain the robot to move in a strictly horizontal plane.

3. Modeling of Underwater Snake Robots with Added Effectors

This section briefly presents two different modeling approaches proposed for underwater snake robots with added effectors. These modeling approaches are used as the basis for obtaining simulated results for comparison with experimental results in this paper.

3.1. An Analytical Model for USRs

Several USR models have been proposed in previous studies [22, 23, 24, 25, 26, 27]. A closed-form model for USRs with added effectors was presented in [28], in which both resistive and reactive fluid forces are considered. In particular, the model proposed in [28] considers several hydrodynamic effects, such as linear and nonlinear drag forces, the added mass effect, fluid moments and current effects. This model is general in the sense that it can be used to simulate the behavior of snake robots with added effectors moving on land or swimming in the water by considering either a ground friction model [29] or a fluid friction model [28]. In this section, we briefly present the equations of motion for a USR with added effectors since they will be used in the following sections to obtain simulated results for comparison with the physical robot Mamba with regard to the locomotion efficiency of USRs. For more details, see [28].

In [28], it is shown that the equations of motion for a USR with links of different masses and lengths can be expressed as follows:

$$\begin{aligned}
\begin{bmatrix} \ddot{p}_x \\ \ddot{p}_y \end{bmatrix} &= -\mathbf{M}_p \mathbf{N}_p \begin{bmatrix} \text{diag}(\dot{\theta}) & \mathbf{0} \\ \mathbf{0} & \text{diag}(\dot{\theta}) \end{bmatrix} \mathbf{E} \begin{bmatrix} \dot{p}_x \\ \dot{p}_y \end{bmatrix} \\
&- \mathbf{M}_p \mathbf{N}_p \begin{bmatrix} \text{diag}(\dot{\theta}) & \mathbf{0} \\ \mathbf{0} & \text{diag}(\dot{\theta}) \end{bmatrix} \begin{bmatrix} \bar{\mathbf{K}}^T \mathbf{S}_\theta \dot{\theta} - \mathbf{V}_x \\ -\bar{\mathbf{K}}^T \mathbf{C}_\theta \dot{\theta} - \mathbf{V}_y \end{bmatrix} \\
&- \mathbf{M}_p \mathbf{L}_p \begin{bmatrix} \bar{\mathbf{K}}^T (\mathbf{C}_\theta \dot{\theta}^2 + \mathbf{S}_\theta \ddot{\theta}) \\ \bar{\mathbf{K}}^T (\mathbf{S}_\theta \dot{\theta}^2 - \mathbf{C}_\theta \ddot{\theta}) \end{bmatrix} + \mathbf{M}_p \mathbf{E}^T \begin{bmatrix} \mathbf{f}_{Dx} + \mathbf{f}_{tx} \\ \mathbf{f}_{Dy} + \mathbf{f}_{ty} \end{bmatrix},
\end{aligned} \tag{1}$$

$$\begin{aligned}
&\mathbf{M}_\theta \ddot{\theta} + \mathbf{W}_\theta \dot{\theta}^2 + \mathbf{V}_{\theta, \dot{\theta}} \dot{\theta} + \mathbf{N}_{\theta, \dot{\theta}} (\mathbf{e} \dot{p}_x - \mathbf{V}_x) + \mathbf{P}_{\theta, \dot{\theta}} (\mathbf{e} \dot{p}_y - \mathbf{V}_y) \\
&+ \mathbf{K}_x (\mathbf{f}_{Dx} + \mathbf{f}_{tx}) + \mathbf{K}_y (\mathbf{f}_{Dy} + \mathbf{f}_{ty}) - \boldsymbol{\tau}_t = \mathbf{D}^T \mathbf{u},
\end{aligned} \tag{2}$$

where $\dot{\theta}^2 = [\dot{\theta}_1^2, \dots, \dot{\theta}_n^2]^T$ and (p_x, p_y) represents the global coordinates of the center of mass (CM) of the robot; the parameters $\theta \in \mathbf{R}^n$ represent the link angles, where n is the number of links of the robot; and $\mathbf{V}_x = \mathbf{e}V_x \in \mathbf{R}^n$ and $\mathbf{V}_y = \mathbf{e}V_y \in \mathbf{R}^n$, where V_x and V_y are the ocean current velocities in the inertial x and y directions, respectively. The vectors $\mathbf{f}_{Dx} = \mathbf{f}_{Dx}^I + \mathbf{f}_{Dx}^{II}$ and $\mathbf{f}_{Dy} = \mathbf{f}_{Dy}^I + \mathbf{f}_{Dy}^{II}$ represent the drag forces in the x and y directions, and the vectors $(\mathbf{f}_{tx}, \mathbf{f}_{ty})$ and $\boldsymbol{\tau}_t$ represent the forces and torques, respectively, acting on the links due to the added effectors. The vector $\mathbf{u} \in \mathbf{R}^{n-1}$ is the control input, and the analytical expressions for the following vectors and matrices can be found in [28]: $\bar{\mathbf{K}}$, \mathbf{S}_θ , \mathbf{C}_θ , \mathbf{e} , \mathbf{E} , \mathbf{M}_p , \mathbf{N}_p , \mathbf{L}_p , \mathbf{M}_θ , \mathbf{W}_θ , $\mathbf{V}_{\theta, \dot{\theta}}$, $\mathbf{N}_{\theta, \dot{\theta}}$, $\mathbf{P}_{\theta, \dot{\theta}}$, \mathbf{K}_x and \mathbf{K}_y .

3.2. A USR Model in Vortex

In addition to the analytical model presented in the previous subsection, this paper proposes to use a simulation software as a second way of modeling an underwater snake robot. In particular, models for underwater snake robots with and without added effectors in a complete 3D simulation environment created by using the software Vortex are presented. In this paper, Vortex model is mainly used to validate the analytical model presented in the previous subsection to obtain an accurate model with which to compare simulated and experimental results regarding the locomotion efficiency of USRs with and without added effectors, as reported in Section 4. In Fig. 2a and Fig. 2b, the models of the two different configurations of Mamba developed in the Vortex environment are shown.

Vortex is a simulation software created by CM Labs [30] that provides a 3D environment with realistic physics suitable for both modeling and simulating various mechanisms. In addition to providing a dynamics engine for land-based mechanisms, Vortex also supports marine simulations. In Vortex, the first step of the modeling process is to create a graphical representation of the model. The approach that is adopted in this paper is to create the graphical representation of the model in SolidWorks and then import this graphical model into Vortex. When a graphical model is imported into Vortex, it is transformed into Vortex's native graphics representation format, known as Graphics Gallery. Once the desired Graphics Gallery has been acquired, the next step is to create a new mechanism and insert the Graphics Gallery into it. The Graphics Gallery will

175 contain nodes representing each part of the model. From these nodes, it is possible to
create Vortex parts. Note that these parts define the actual physical properties of the
model, whereas their geometry is defined by the graphics node from which each part
was created. Afterward, the corresponding physical properties, such as the mass, inertia
and added mass, can be set for the different parts of the model. Although each part
of the model now has both a defined geometry and defined physical properties, they
180 still do not have contact surfaces; this can be addressed by creating a collision geometry
for each part. Note that Vortex has a built-in functionality for creating collision
geometries in the form of convex meshes that wrap around the graphical geometries.
Finally, all parts are connected to form the complete model.

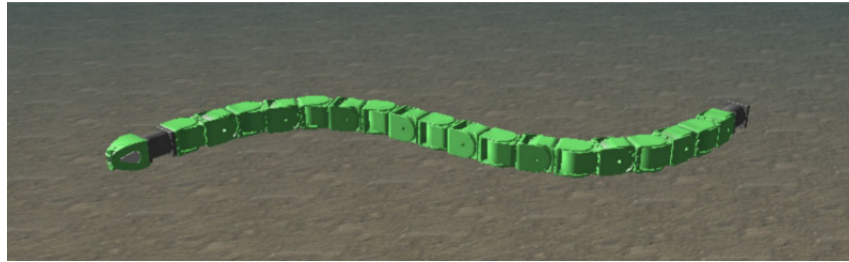
Simulink was used to control the underwater snake robot model in Vortex, as the
185 Vortex software facilitates direct two-way communication with Simulink. The communication
is unfortunately limited to exchanging simulation state data, and does not support
control flow signals. The implication of this is that each simulation would have to
be controlled manually. To overcome this limitation the Vortex software development
kit (SDK) was used to write a python script that controls the Vortex simulation.
190 Similarly a Matlab script was created to control the Simulink part of the simulation.
By having the two scripts communicate through a TCP connection full control of the
simulation process was achieved.

In this paper, the fluid forces modeled using Vortex are nonlinear drag forces, added
mass forces and current forces. The obtained Vortex simulation environment for USRs
195 is thus regarded as suitable software for modeling a USR because it provides a relatively
accurate hydrodynamic model while permitting real-time visualization, which provides
valuable insight into the USR dynamics. The fact that the simulations are run in
real time also makes it feasible to run many simulations for the purpose of parameter
identification. The following section describes the use of the developed Vortex model
200 of USRs with and without added effectors to obtain fluid parameters for the analytical
model. By performing a comparative analysis between the simulated Vortex model and
the analytical model, we will show that it is possible to ensure that both the analytical
model and the Vortex model yield accurate representations of the snake robot's dynamics.
Note that since both the Vortex model and the analytical model are shown to be
205 accurate, they can be used together with the experimental results when investigating
the locomotion efficiency of USRs with and without added effectors, as reported in
Section 4

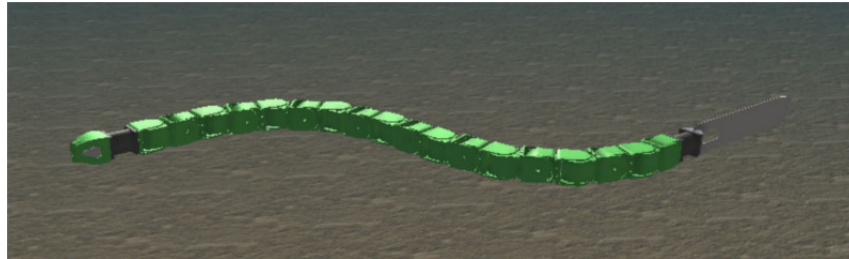
4. Experimental Study

This section describes the experimental setup employed to investigate the locomotion
210 efficiency and path-following of USRs with added effectors. In particular, it presents
experimental results for fluid parameter identification, locomotion efficiency and
straight-line path-following for Mamba with and without a passive caudal fin, using
both lateral undulation and eel-like motion patterns.

In Section 3, two different modeling concepts for the locomotion of underwater
215 snake robots were proposed, both of which can describe the hydrodynamics of a USR
quite accurately. Although the precision is far from that of a full computational fluid
dynamics (CFD) simulation, we will show in the following subsections that the adopted



(a) Mamba without added effectors.



(b) Mamba with a caudal fin.

Figure 2: Models of the underwater snake robot Mamba in the Vortex simulation environment.

220 concepts are sufficient to describe the dynamics of USRs and enable real-time simu-
 lations of the behavior of such robots. Note that in [21], the efficiency of the USR
 Mamba without added effectors was investigated for both lateral undulation and eel-
 like motion patterns. Similar studies were presented in [18], where the effect of adding
 a tail thruster module to Mamba was analyzed. This paper reports additional experi-
 ments conducted in a manner similar to those described in [8, 18] to obtain data for
 quite a wide range of gait parameters for two different configurations of Mamba, with
 225 and without a caudal fin.

4.1. Experimental Setup

230 The experiments were performed in a tank with dimensions of $L=40$ m, $H=1.5$ m
 and $W=6.45$ m in the MC-lab at NTNU [31]. An underwater camera positioning sys-
 tem consisting of six cameras from Qualisys [32] was used to obtain real-time position
 and orientation measurements. Specifically, it recorded the position and orientation of
 an attachment on the last module consisting of five underwater reflective markers, as
 shown in Fig. 1b. The coverage volume of the installed underwater camera system had
 dimensions of $12\text{ m} \times 1.35\text{ m} \times 5.45\text{ m}$, which were sufficient for the experimental trials
 presented in this paper. Note that the markers were submerged at a depth of approx-
 235 imately 0.15 m to avoid reflections and thus ensure accurate measurements, since the
 experiments were performed near the water surface. Afterward, the obtained global-
 frame measurements of the position and orientation of the last module were combined
 with the measured joint angles to calculate the center-of-mass position and link angles
 of the robot based on the kinematic equations. See [8] for more details.

240 *4.2. Locomotion Efficiency*

An interesting control problem for USRs concerns the ability to achieve efficient motion, preferably with minimum energy consumption, to allow the robot to undertake longer missions. The locomotion efficiency of USRs has been previously studied in the literature. A discussion of various concepts studied for locomotion efficiency can be found in [21, 33]. However, in all previous studies, only quantitative comparisons were possible regarding the locomotion efficiency of USRs due to the lack of precise fluid parameter identification. In this paper, we present results for the locomotion efficiency of USRs that enable both qualitative and quantitative comparisons between the simulated results and those observed for the physical robot Mamba.

Note that for biologically inspired USRs, propulsion is commonly achieved through the interaction of the body with the surrounding water during body undulations. Hence, in this paper, we consider the general sinusoidal motion pattern introduced in [34], in which each joint $i \in \{1, \dots, n-1\}$ of the robot follows a sinusoidal reference signal:

$$\phi_i^{\text{ref}}(t) = \alpha g(i, n) \sin(\omega t + (i-1)\delta) + \phi_0, \quad (3)$$

250 where body undulations of constant amplitude (i.e., lateral undulation, with $g(i, n) = 1$) or of increasing amplitude from the head to the tail (i.e., eel-like motion, with $g(i, n) = (n-i)/(n+1)$) can be achieved by properly selecting the scaling function $g(i, n)$. In this expression for the sinusoidal motion pattern, α , ω and δ denote the maximum amplitude, the frequency and the phase shift between the joints, respectively, and the phase offset ϕ_0 can be used to induce a turning motion [29, 35].

255 For the experimental trials of locomotion efficiency presented in this paper, the average power consumption was calculated using the following equation:

$$P_{\text{avg}} = VI_{\text{avg}} - VI_0, \quad (4)$$

where $V = 35$ V and I_{avg} is the average current measured using a FLUKE 289 multimeter, which is able to measure average, maximum and minimum current values. Specifically, the FLUKE 289 was attached to the power box that was connected to the power supply cable for Mamba during the experiments. An initial average current value of $I_0 = 1.18$ A was measured by the multimeter before the application of the reference joint angles to the robot, and this value was subtracted from the total average power consumption. Note that in this way, we eliminated the contribution to the power consumption from the electronics inside the joint modules at rest to obtain more precise comparisons regarding the power consumption.

For each trial in both the simulations and the experiments, the average forward velocity was calculated as

$$\bar{v}_t = \frac{\sqrt{(p_{\text{stop},x} - p_{\text{start},x})^2 + (p_{\text{stop},y} - p_{\text{start},y})^2}}{t_{\text{stop}} - t_{\text{start}}}, \quad (5)$$

265 where the positions $\mathbf{p}_{\text{start}}$ and \mathbf{p}_{stop} denote the starting and ending points of the CM of the robot (i.e., the difference between them is the distance traveled by the CM of the robot).

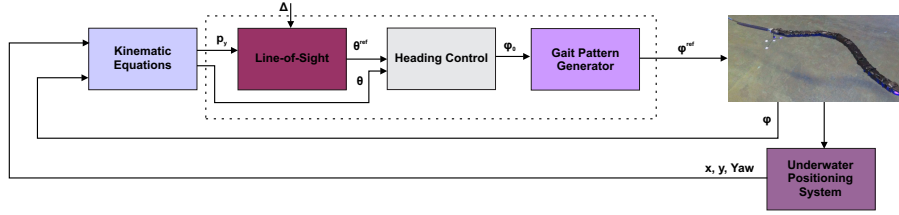


Figure 3: Illustration of the path-following control approach for underwater snake robots.

4.3. Path-Following

Several control approaches for USRs have been proposed in the literature [8, 22, 36, 37, 38]. A discussion of the different path-following approaches proposed for USRs can be found in [8, 37]. In this section, we briefly introduce the line-of-sight (LOS) path-following control approach presented in [8] for USRs. This approach was applied in this study for a USR with a passive caudal fin to investigate the convergence to the straight-line path, the achieved forward velocity, and the power consumption. The structure of the path-following control approach is shown in Fig. 3. This control approach consists of a LOS guidance law responsible for producing the reference heading (orientation), a heading controller responsible for making the actual heading follow the desired one, and a gait pattern generator that produces the required undulatory motion to propel the robot forward. The control objective of the path-following approach is to make the robot converge to the desired straight-line path with a nonzero forward velocity. The desired path is aligned with the global x axis, and the actual heading of the robot is calculated as the average of the horizontal link angles as follows:

$$\theta = \frac{1}{n} \sum_{i=1}^n \theta_i. \quad (6)$$

The following LOS guidance law [39] is used to define the desired heading θ_{ref} of the robot as a function of the position p_y of the center of mass (CM) of the robot along the global y axis (i.e., the cross-track error):

$$\theta_{\text{ref}} = -\arctan\left(\frac{p_y}{\Delta}\right), \quad \Delta > 0, \quad (7)$$

where Δ is a design parameter called the *look-ahead distance*, which influences the rate of convergence to the desired path and, thus, the transient motion of the robot [39]. See [8] for more details.

As mentioned earlier, the joint angle offset ϕ_0 is used for the directional control of the underwater snake robot. In this study, the following simple P-controller was used to make the actual heading, θ , follow the desired one, θ_{ref} :

$$\phi_0 = k_\theta (\theta_{\text{ref}} - \theta), \quad (8)$$

where $k_\theta > 0$ is a control gain [8].

4.4. Fluid Parameter Identification

In this section, we present the results obtained regarding fluid parameter identification for the underwater snake robot Mamba with and without a passive caudal fin. The fluid coefficients to be identified are the drag coefficients in the x and y directions of motion, C_f and C_D , respectively, and the added mass coefficient, C_A . Note that the added mass inertia coefficient is commonly set to the theoretical value of $C_M = 1$ since this parameter does not significantly affect the overall motion of the system [8, 26, 40].

For the analytical model, we adopted in this study the values of the coefficients obtained in [8]. In [8], it was shown that by performing a back-to-back comparison of experimental data and ideal simulation results, it is possible to find the fluid coefficients through curve fitting between one set of simulated data and one set of data from the motion of the physical robot Mamba. In [8], the identified fluid coefficients were $C_f = 0.3$, $C_D = 1.75$, and $C_A = 1.5$ for lateral undulation and $C_f = 0.17$, $C_D = 1.75$, and $C_A = 1.5$ for eel-like motion. The comparisons between the simulated and experimental results presented in the following subsection of this paper for wide ranges of the gait parameters α , ω and δ show that the fluid coefficients obtained in [8] can be used to accurately model USRs since they provide results regarding the achieved forward velocity that are both quantitatively and qualitatively similar to the experimental observations.

The same fitting approach proposed in [8] was adopted in this study to obtain the fluid coefficients for the presented Vortex model. Specifically, back-to-back curve fitting between the simulated behavior and the experimentally observed behavior of the physical robot Mamba was performed for different values of the gait parameters. The obtained fluid parameters for the Vortex model are $C_f = 0.1$, $C_D = 0.3$ and $C_A = 1.27$. Note that the fluid parameters identified for the analytical model and the Vortex model have different values; this is expected since in both cases, simplifications have been made regarding the hydrodynamic effects. In addition, the Vortex model is able to model only nonlinear drag effects, whereas in the analytical model, both linear and nonlinear drag forces are captured. However, we will see in the following subsections that by using the obtained fluid parameters, we are able to achieve accurate agreement between the motion of the simulated models and the motion of the physical robot, Mamba. This indicates that both the analytical and Vortex modeling approaches with the obtained fluid coefficients can be used to study the behavior of USRs and to investigate the suitability of different control approaches for USRs in the future. In addition, the findings show that the models presented in this paper are valid and suitable for the analysis and control of USRs.

4.5. Experimental Results: Locomotion Efficiency

In this section, we present the simulated and experimental results for the locomotion efficiency study using the underwater snake robot Mamba with and without a passive caudal fin for the two most common motion patterns for underwater snake robots: lateral undulation and eel-like motion.

Experimental results were obtained for a) varying α and constant ω and δ , b) varying ω and constant α and δ and c) varying δ and constant α and δ for the two different configurations of the robot using the two different motion patterns. The investigated

ranges of the gait parameters are shown in the corresponding figures. To study the influence of the gait parameters α , ω and δ on the snake robot's locomotion efficiency, experiments were conducted at different values of the gait parameters. In addition,

 320 simulations were performed to replicate the experimental trials that were conducted, and the simulated results are also presented in this section. During each simulation, the USR was initially straight and lying still (i.e., with all joint angles equal to zero and the velocity equal to zero) in the horizontal xy plane along the x axis with its head pointing in the positive x direction. When the simulation was started, the USR was actuated by

 325 applying a control signal consistent with either lateral undulation or eel-like motion. The gait parameters were kept constant throughout each simulation. The simulation time was 30 s, identical to the experimental case, during which all joint angles as well as the CM position and orientation were measured. Simulations were performed for different sets of gait parameters depending on the motion pattern and the USR configuration (with or without a caudal fin). The measured data from the simulations were

 330 then used to calculate the average forward velocity of the robot.

Fig. 4-7 show the results regarding the achieved forward velocity from the analytical model (\bar{v}_i^m), the Vortex model (\bar{v}_i^v), and three sets of experimental trials performed to demonstrate the repeatability of the experimental results (\bar{v}_{i_1} , \bar{v}_{i_2} , and \bar{v}_{i_3}) as well as

 335 the average value of the forward speed calculated based on the values obtained during the three trials (\bar{v}_i^e). Fig. 4a and 5a and Fig. 6a and 7a show the average forward velocities for different values of the gait parameter α while ω and δ are kept constant for the lateral undulation and eel-like motion patterns, respectively. Fig. 4b and 5b and Fig. 6b and 7b show similar results for different values of ω , and Fig. 4c and 5c and Fig. 6c and 7c for different values of δ . From Fig. 4, we can see very good quantitative and qualitative agreement between the simulated results and the behavior of the physical robot for the investigated ranges of the gait parameters α , ω and $\delta \in [35, 50]$ for the lateral undulation motion pattern for the USR configuration without a caudal fin. Note that the simulations with varying α and ω were conducted with a constant

 345 $\delta = 40^\circ$, which is within this region. One notable difference between the simulated and experimental results is that the value of δ at which Mamba reaches its maximum velocity, δ_{max} , is vastly different. For instance, in Fig. 4c we see that δ_{max} is 25° and 35° for the simulated and the physical robot, respectively, meaning that δ_{max} is in the magnitude of 10o. However, in theoretical studies [21], it has been found that the value of δ_{max} depends on many parameters and not the fluid coefficients alone. Considering this fact, it might not be possible to achieve the correct δ_{max} by varying only the fluid coefficients. It must also be mentioned that the experimental results for varying δ suffer from fewer data points.

Remark 1. *Note that during the experiments, the USR Mamba swam along the surface, which might have resulted in some hydrodynamic effects that would not be present

 355 if the robot were fully submerged. Another point worth mentioning is that during the experiments, Mamba had a tether connected to its tail for the supply of power and the transmission of the control signals, whereas this tether was not present in the simulations. At high velocities, the effects of swimming at the surface and of the tether might

 360 have been more dominant, resulting in a lower velocity than would have been the case if the USR were fully submerged and untethered, as in the simulations.*

Fig. 4 shows that for all investigated cases, there is good quantitative agreement between the behavior of the simulated robot and the physical robot with a caudal fin. In addition, it shows that the behavior of the robot simulated in Vortex is closer to that of the physical robot as observed during the experiments than the analytical model. Considering that the fluid parameter identification was performed using only the experimental data from the case without a caudal fin, the results were expected to be less accurate in terms of quantitative similarity. In addition, note that the caudal fin attached to the physical robot was flexible. During swimming, the elastic nature of the caudal fin should have generated additional fluid forces that directly contributed to the forward propulsion. Furthermore, it should be considered that the elasticity of the experimental caudal fin might also have produced additional hydrodynamic effects such as vortices that could also have contributed to the forward motion. In the analytical and Vortex model, however, the caudal fin was modeled as a rigid object, meaning that any effects arising from the elastic nature of the caudal fin in the experiments were not present in the simulations. Fig. 6 and 7 show good agreement between the simulated and experimentally obtained results, which are both quantitatively and qualitatively similar, when the eel-like motion pattern was used. Note that when the USR moves in an eel-like motion pattern, the front part of its body oscillates with a smaller amplitude than the hind part, resulting in less drag force in the direction of the body than when the entire body oscillates with the same amplitude, as is the case during lateral undulation motion. In the simulation models, this effect was not present since all parts of the robot were modeled with the same fluid coefficients. In the future, both the elasticity of the caudal fin and the lower drag resulting from the eel-like motion pattern should be included in the simulation models to obtain results that are even more quantitatively similar. Note that all of the results presented in this paper validate the theoretical findings in [21], and in addition, by performing extensive fluid parameter identification, we were able to obtain both qualitatively and quantitatively similar results between the simulations and experiments over quite wide ranges of the investigated gait parameters.

In Fig. 8-11, the power consumption is shown for all investigated cases. Note that in this paper, we do not present simulated results regarding the power consumption since the analytical and Vortex model do not capture the influence of the motors, electronics and joint actuators, which directly affect the power consumption. However, the experimental results presented in this paper for the power consumption show very good agreement with the trend exhibited by the theoretical results obtained in [21].

Table 1 shows the maximum values of the achieved forward velocity and the corresponding power consumption for each case investigated in Fig. 4-7 by considering different values of the gait parameters α , ω and δ for both the lateral undulation and the eel-like motion pattern. In particular, for the results shown in each figure we present in Table 1 the maximum forward velocity, the corresponding power consumption and the values of the gait parameters for the maximum forward velocity indicated as α_{max} , ω_{max} and δ_{max} for the two investigated motion patterns with and without a caudal fin. From Table 1, we see that for the same values of the gait parameters, we can achieve an increase of 47.03% to 82.95% for lateral undulation and 33.64% to 88.68% for eel-like motion pattern in the forward velocity by simply attaching a passive caudal tail to the robot. Furthermore, from Table 1 we see that the power consumption has even decreased in most of the cases by simply attaching a caudal fin to the robot. Note that

the experimental results presented in this paper furthermore indicate that the properties derived and experimentally validated in [21] for an underwater snake robot without a caudal fin also hold for an underwater snake robot with a passive caudal fin. In particular, the results presented in [41] indicate that by increasing the length of the robot by 100 % (i.e., increasing the number of links from 10 to 20), it is possible to increase the forward velocity only by less than 20 % for both lateral undulation and eel-like motion. By contrast, we see here that by attaching a passive caudal fin, which results in a 30 % increase in the total length of the robot, we achieve an increase of almost 100 % in the forward velocity. At the same time, the results in Table 1 show that the average power consumption is decreased in most of the investigated cases. By contrast, doubling the number of links would increase the average power consumption by almost a factor of 10 [41] while only resulting in a less than 20 % increase in the forward velocity. The experimental results thus indicate that a passive fin provides increased locomotion efficiency.

Remark 2. *Note that the results presented in Fig. 4-7 are promising since they indicate that the Vortex model can be regarded as relatively accurate representations of real-world USRs. In addition, based on the experimental results, we can conclude that for a certain set of chosen fluid coefficients and gait parameters, the simulation models accurately represent the physical robot. This makes these simulation models powerful tools for the visualization and testing of new control algorithms. Furthermore, for the set of fluid coefficients obtained from the system identification in [8], the analytical model produces the same results as the corresponding Vortex simulation model. This implies that the analytical model can be used for the model-based control of simulated robots. Since both the Vortex and the analytical models have been shown to accurately represent the physical robot, this further implies that the analytical model can be used for the model-based control of the real robot. Having a sufficiently accurate analytical model of the system will enable the development of a wide range of controllers; thus, it is concluded that designing a fully autonomous USR based on the analytical model could be feasible in the future.*

Remark 3. *Note that in this study, the analytical and Vortex model were tuned based on the curve-fitting approach described in [8] to qualitatively and quantitatively match the experimental data for the case of Mamba without any added effectors swimming with the lateral undulation motion pattern. Hence, the simulated results presented for the cases with a caudal fin are less accurate with regard to their quantitative similarity to the results for the physical robot. However, we can see from Fig. 4-7 that overall, the results agree quite well with respect to both qualitative and quantitative criteria. Alternative methods for fluid parameter identification considering different configurations of the robot and the influence of the gait patterns could be investigated in the future to achieve even greater accuracy.*

4.6. Experimental Results: Path-Following

In this section, we compare the experimental results obtained for the path-following behavior of the USR Mamba with and without a passive caudal fin for the two most

Table 1: Comparison of locomotion efficiency results for USRs with and without a passive caudal fin. NA stands for not available measurements from the experiments due to device failures or different range of gait parameters choice for different gait patterns.

	α [deg]	ω [deg/s]	δ [deg]	max \bar{v}_l [m/s]	P_{avg} [W]	% change on \bar{v}_l	% change on P_{avg}
Lateral undulation without a passive caudal fin							
Case 1	30	$\omega_{max}=130$	40	0.1514	106.63		
Case 2	30	150	40	0.1436	123.52		
Case 3	$\alpha_{max}=36$	110	40	0.1361	95.68		
Case 4	30	110	20	NA	NA		
Case 5	30	110	$\delta_{max}=35$	0.1529	105.35		
Lateral undulation with a passive caudal fin							
Case 1	30	130	40	0.2226	102.67	47.03%	-3.71%
Case 2	30	$\omega_{max}=150$	40	0.2461	114.29	71.38%	-7.47%
Case 3	$\alpha_{max}=36$	110	40	0.2490	100.26	82.95%	10.11%
Case 4	30	110	$\delta_{max}=20$	0.2654	173.58	-	-
Case 5	30	110	35	0.2266	100.86	48.20%	-4.26%
Eel-like motion without a passive caudal fin							
Case 1	30	$\omega_{max}=130$	40	0.1132	NA		
Case 2	30	150	40	0.0945	NA		
Case 3	$\alpha_{max}=48$	110	40	0.1302	93.37		
Case 4	50	110	40	0.1291	88.24		
Case 5	30	110	20	NA	NA		
Case 6	30	110	$\delta_{max}=35$	0.1132	99.21		
Eel-like motion with a passive caudal fin							
Case 1	30	130	40	0.1725	90.45	52.39%	-
Case 2	30	$\omega_{max}=150$	40	0.1783	83.01	88.68%	-
Case 3	48	110	40	0.1740	89.32	33.64%	-4.34%
Case 4	$\alpha_{max}=50$	110	40	0.2018	90.07	56.31%	2.07%
Case 5	30	110	$\delta_{max}=20$	0.1785	119.54	-	-
Case 6	30	110	35	0.1619	89.60	43.02%	-9.69%

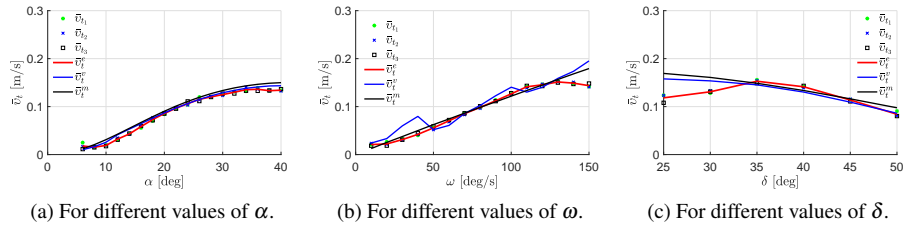


Figure 4: Forward velocity of the USR without a caudal fin swimming with the lateral undulation motion pattern.

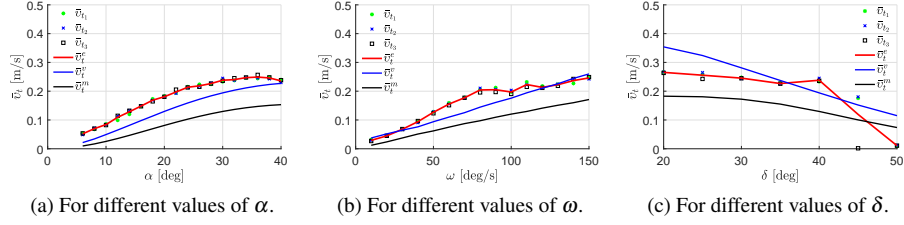


Figure 5: Forward velocity of the USR with a caudal fin swimming with the lateral undulation motion pattern.

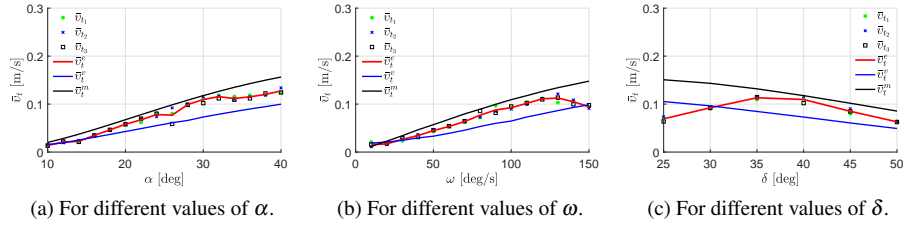


Figure 6: Forward velocity of the USR without a caudal fin swimming with the eel-like motion pattern.

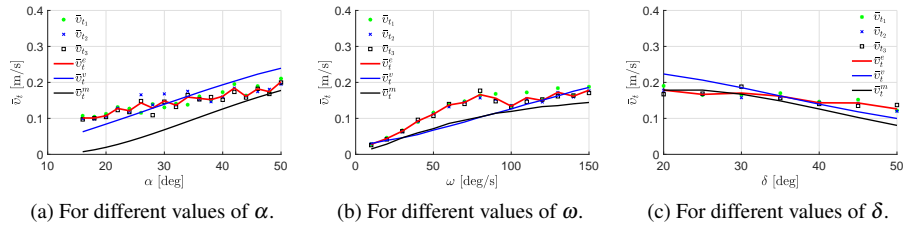


Figure 7: Forward velocity of the USR with a caudal fin swimming with the eel-like motion pattern.

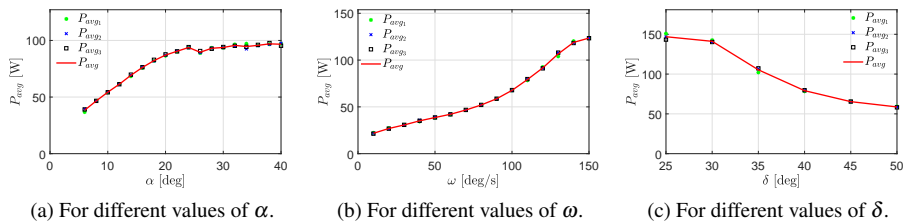


Figure 8: Power consumption of the USR without a caudal fin swimming with the lateral undulation motion pattern.

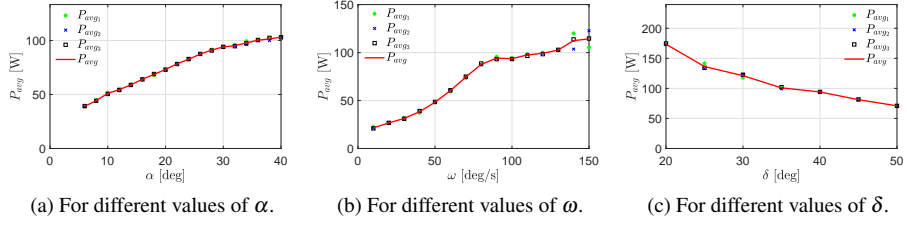


Figure 9: Power consumption of the USR with a caudal fin swimming with the lateral undulation motion pattern.

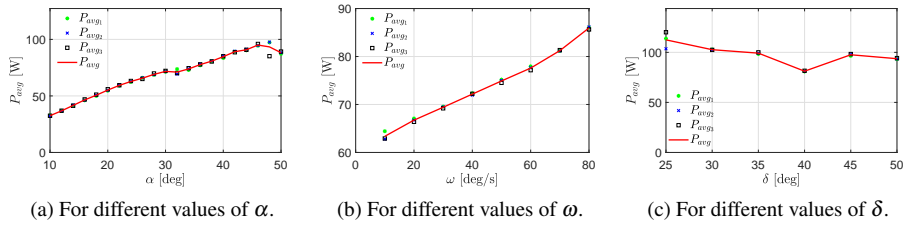


Figure 10: Power consumption of the USR without a caudal fin swimming with the eel-like motion pattern.

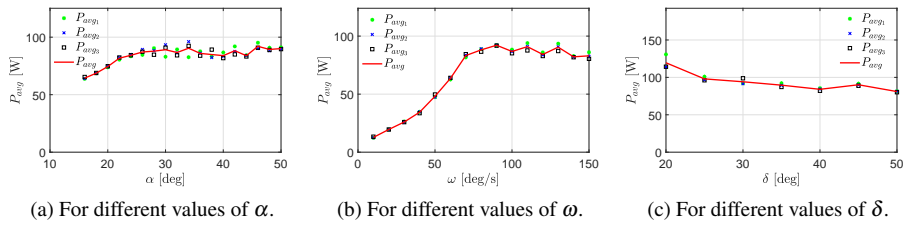


Figure 11: Power consumption of the USR with a caudal fin swimming with the eel-like motion pattern.

450 common motion patterns for underwater snake robots: lateral undulation and eel-like motion. For each trial, results were obtained for three different sets of initial positions and orientations of the robot. An illustration of the experimental setup is shown in Fig. 3. The LOS path-following approach was implemented on an external computer. The general sinusoidal motion pattern was calculated based on (3), and the reference joint angles were sent to each joint through the CAN bus. For the path-following control approach, constant values were chosen for the parameters α , ω and δ , whereas the parameter ϕ_0 was used for directional control. Note that during these experimental trials, a P-controller implemented at a low level (i.e., in the microcontroller of each module) was responsible for making the joint angles follow the reference angles since 460 the servos used in Mamba do not permit joint torque control.

The calculations for the LOS path-following control approach described in (6)-(7) were performed with a look-ahead distance of $\Delta = 0.18$ and a control gain of $k_\theta = 0.4$ for all experimental trials, as shown in Table 2, for both lateral undulation and eel-like motion. The gait parameters of the sinusoidal motion pattern were set to $\delta = 40^\circ$ and 465 $\omega = 90^\circ/\text{s}$ for both patterns and to $\alpha = 30^\circ$ and 40° for lateral undulation and eel-like motion, respectively. Note that during the trials, the joint offset $\phi_0 = [-20^\circ, 20^\circ]$ was saturated to account for the physical constraints on the joint angles of Mamba. In each trial, the robot's joint angles were initially set to zero. Comparisons of the average forward velocity and average power consumption results for all of the different trials are shown in Table 2. The initial heading and position of the center of mass of the robot 470 for each trial are shown in Table 2. Fig. 12-14 and Fig. 15-17 present the experimental results obtained using Mamba with and without a passive caudal fin, respectively, for the lateral undulation motion pattern. Similar results from all trials for the eel-like motion pattern are shown in Fig. 18-23.

475 As we can see from Fig. 12a-23a, the robot successfully reached and followed the desired straight-line path in all trials with different initial conditions for both lateral undulation and eel-like motion patterns. In addition, it can be easily seen from Fig. 12b-23b that the cross-track error, as expected, converged toward and oscillated around zero and from Fig. 12c-23c that the heading controller successfully ensured that the actual heading followed the reference in all investigated cases. However, by comparing 480 Fig. 12-14 with Fig. 15-17, we can see that the convergence to the path was much faster for the configuration with a passive caudal fin. In particular, the robot with a passive caudal fin managed to achieve almost double the forward speed (i.e., a 100 % increase in the forward velocity) compared with the robot without a caudal fin, as also seen in 485 Table 2.

Another interesting observation is that the achieved forward velocity and the average power consumption are of the same order of magnitude among all trials with different initial positions. Note that during each trial, the gait parameters α , ω and δ were constant. In [21], it was shown that the forward velocity and the power consumption directly depend on the gait parameters for the free-swimming case (i.e., open loop control). Hence, we can conclude that the forward speed and the power consumption are independent of the initial conditions since we maintained the same values of the gait parameters α , ω and δ , the look-ahead-distance Δ and the control gain K_θ in all cases. This means that by choosing proper values of these parameters, we can achieve open- 495 loop control of the forward velocity and the power consumption, which is consistent

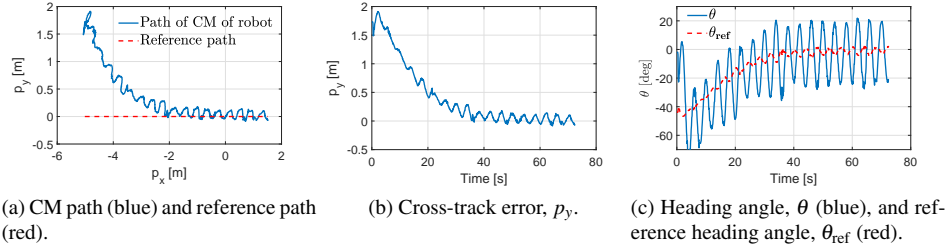


Figure 12: Case 1 for lateral undulation: Straight-line path-following of the physical snake without a caudal fin with the initial distance from the CM being $p_y = 1.7352$ m.

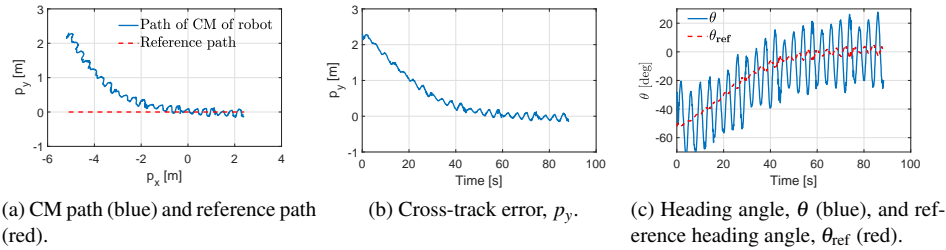


Figure 13: Case 2 for lateral undulation: Straight-line path-following of the physical snake without a caudal fin with the initial distance from the CM being $p_y = 2.2867$ m.

with the theoretical results obtained based on averaging theory as well as the simulated and experimental results presented in [21]. Note that this finding is also consistent with the properties derived in [21] based on averaging theory for USR locomotion without closing the control loop.

500 **5. Conclusions and Future Work**

In this paper, experimental results have been presented for the locomotion efficiency and path-following control of the bioinspired underwater snake robot Mamba

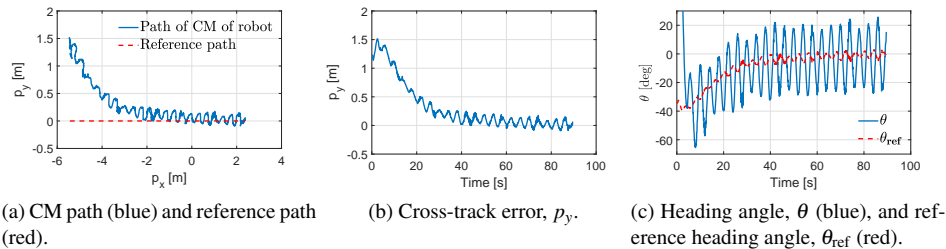


Figure 14: Case 3 for lateral undulation: Straight-line path-following of the physical snake without a caudal fin with the initial distance from the CM being $p_y = 1.2235$ m.

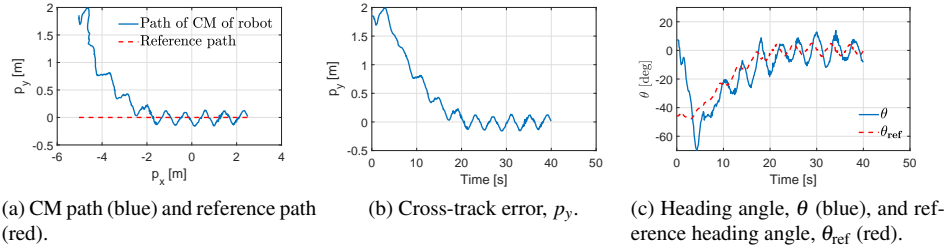


Figure 15: Case 1 for lateral undulation: Straight-line path-following of the physical snake with a caudal fin with the initial distance from the CM being $p_y = 1.848$ m.

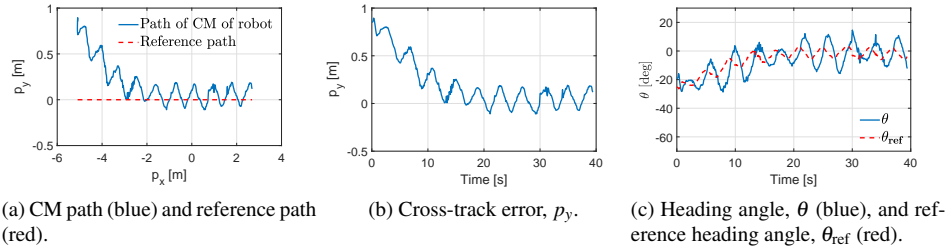


Figure 16: Case 2 for lateral undulation: Straight-line path-following of the physical snake with a caudal fin with the initial distance from the CM being $p_y = 0.8515$ m.

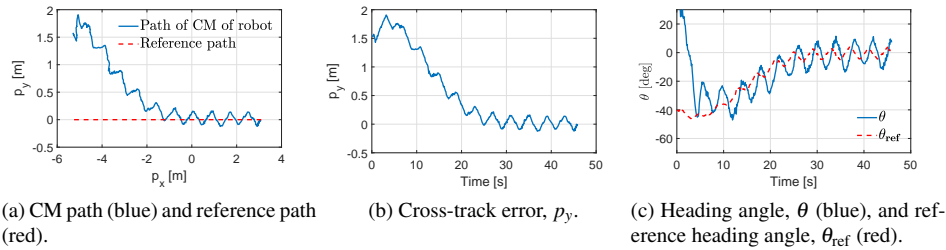


Figure 17: Case 3 for lateral undulation: Straight-line path-following of the physical snake with a caudal fin with the initial distance from the CM being $p_y = 1.5344$ m.

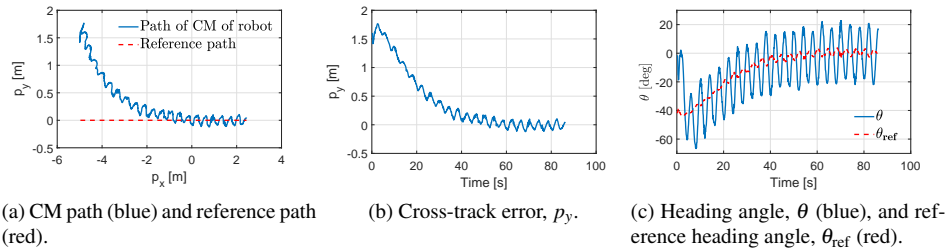


Figure 18: Case 1 for eel-like motion: Straight-line path-following of the physical snake without a caudal fin with the initial distance from the CM being $p_y = 1.5932$ m.

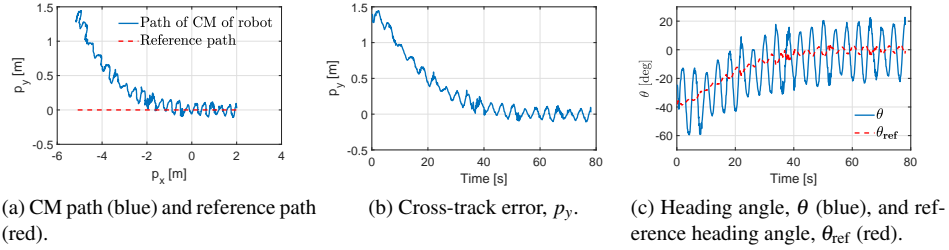


Figure 19: Case 2 for eel-like motion: Straight-line path-following of the physical snake without a caudal fin with the initial distance from the CM being $p_y = 1.3950$ m.

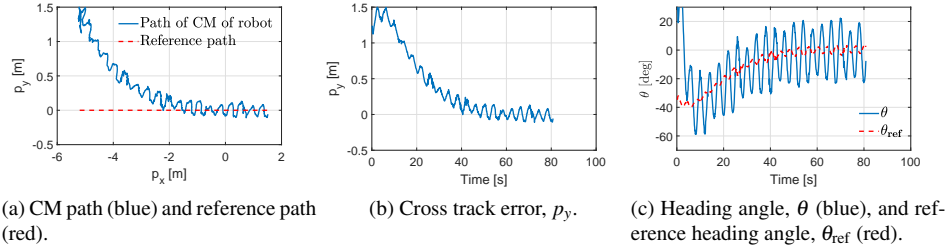


Figure 20: Case 3 for eel-like motion: Straight-line path-following of the physical snake without a caudal fin with the initial distance from the CM being $p_y = 1.2312$ m.

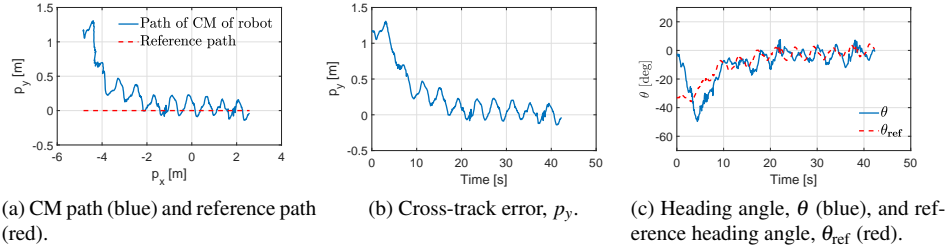


Figure 21: Case 1 for eel-like motion: Straight-line path-following of the physical snake with a caudal fin with the initial distance from the CM being $p_y = 1.1758$ m.

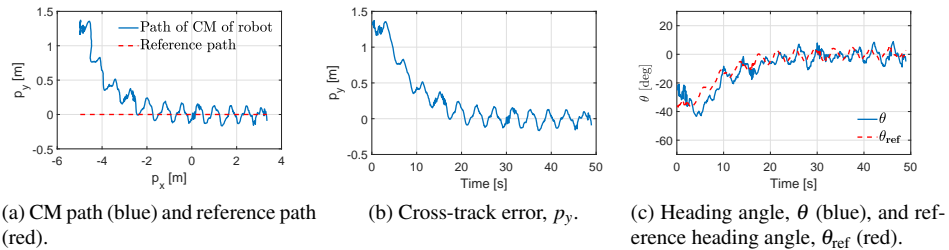


Figure 22: Case 2 for eel-like motion: Straight-line path-following of the physical snake with a caudal fin with the initial distance from the CM being $p_y = 1.3134$ m.

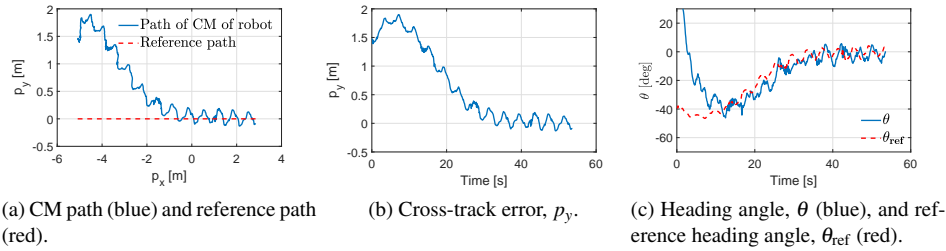


Figure 23: Case 3 for eel-like motion: Straight-line path-following of the physical snake with a caudal fin with the initial distance from the CM being $p_y = 1.4722$ m.

Table 2: Comparison of results for USRs with and without a passive caudal fin.

	Δ [m]	K_θ	θ_0 [deg]	\bar{v}_t [m/s]	P_{avg} [W]	% change on \bar{v}_t	% change on P_{avg}
Lateral undulation without a passive caudal fin							
Case 1	0.18	0.4	-1.86	0.0936	51.77		
Case 2	0.18	0.4	-28.84	0.0892	50.11		
Case 3	0.18	0.4	49.46	0.0883	50.33		
Lateral undulation with a passive caudal fin							
Case 1	0.18	0.4	7.7°	0.1938	97.90	107.05%	89.04%
Case 2	0.18	0.4	-19.06	0.1983	98.60	122.31%	96.76%
Case 3	0.18	0.4	41.49	0.1848	99.30	109.29%	97.29%
Eel-like motion without a passive caudal fin							
Case 1	0.18	0.4	-1.94	0.0878	50.02		
Case 2	0.18	0.4	-24.96	0.0925	50.28		
Case 3	0.18	0.4	36.66	0.0846	51.49		
Eel-like motion with a passive caudal fin							
Case 1	0.18	0.4	-2.76	0.1773	99.51	101.94%	98.94%
Case 2	0.18	0.4	-24.73	0.1724	98.00	86.39%	94.51%
Case 3	0.18	0.4	49.51	0.1510	96.99	78.49%	88.38%

to enable comparisons of its performance with and without a passive caudal fin. Comparative experimental results for the locomotion efficiency were presented for the two most common motion patterns for USRs, lateral undulation and eel-like motion. Based on this comparison, a major advantage of equipping the underwater snake robot with a passive caudal fin, compared with the configuration without any external effectors presented in [8] and the configuration with a tail thruster module presented in [18], is that by simply attaching a passive caudal fin, it is possible to increase the forward velocity by more than 88 % with a relatively low increase or even decrease in power consumption and a minimal increase in the complexity of the mechanical design. An understanding of the differences in locomotion efficiency between USRs with and without passive/active caudal fins could provide new insights for the development of the next generation of bioinspired USRs. In addition, it was shown that a path-following approach previously proposed for underwater snake robots without a caudal fin can be applied for the path-following control of a USR with a caudal fin without any modification. The results presented in this paper demonstrate that this path-following control approach successfully steers the robot toward and along the desired path.

In the future, both the elasticity of the caudal fin and the lower drag resulting from the eel-like motion pattern should be included in the simulation models to obtain results that are even more qualitatively similar. Furthermore, it would be interesting to investigate the locomotion efficiency of USRs with an active caudal fin.

6. Acknowledgments

The authors gratefully acknowledge the engineers in the Department of Engineering Cybernetics, Terje Haugen, Glenn Angell and Daniel Bogen, for implementing the necessary components for the experimental setup as well as Dr. Signe Moe for her contributions in obtaining the experimental results.

7. References

- [1] R. Crespi, A. Badertscher, A. Guignard, A. J. Ijspeert, Amphibot I: an amphibious snake-like robot, *Robotics and Autonomous Systems* 50 (4) (2005) 163–175.
- [2] A. Crespi, A. J. Ijspeert, Amphibot II: An Amphibious Snake Robot that Crawls and Swims using a Central Pattern Generator, in: *Proc. 9th International Conference on Climbing and Walking Robots (CLAWAR)*, Brussels, Belgium, 2006, pp. 19–27.
- [3] M. Porez, F. Boyer, A. J. Ijspeert, Improved lighthill fish swimming model for bio-inspired robots: Modeling, computational aspects and experimental comparisons, *The International Journal of Robotics Research* 33 (10) (2014) 1322–1341.
- [4] C. Stefanini, S. Orofino, L. Manfredi, S. Mintchev, S. Marrazza, T. Assaf, L. Capantini, E. Sinibaldi, S. Grillner, P. Wallen, P. Dario, A novel autonomous, bioinspired swimming robot developed by neuroscientists and bioengineers, *Bioinspiration & Biomimetics* 7 (2) (2012) 025001.

- [5] J. Sverdrup-Thygeson, E. Kelasidi, K. Y. Pettersen, J. T. Gravdahl, Modeling of underwater swimming manipulators, in: Proc.10th IFAC Conference on Control Applications in Marine Systems (CAMS), Trondheim, Norway, 2016, pp. 81–88.
- 545 [6] J. Sverdrup-Thygeson, E. Kelasidi, K. Y. Pettersen, J. T. Gravdahl, A control framework for biologically inspired underwater swimming manipulators equipped with thrusters, in: Proc.10th IFAC Conference on Control Applications in Marine Systems (CAMS), Trondheim, Norway, 2016, pp. 89–96.
- [7] M. Kruusmaa, P. Fiorini, W. Megill, M. De Vittorio, O. Akanyeti, F. Visentin, L. Chambers, H. El Daou, M.-C. Fiazza, J. Jezov, M. Listak, L. Rossi, T. Salumae, G. Toming, R. Venturelli, D. Jung, J. Brown, F. Rizzi, A. Quattieri, J. Maud, A. Liszewski, Filose for svenning: A flow sensing bioinspired robot, IEEE Robotics Automation Magazine 21 (3) (2014) 51–62.
- 550 [8] E. Kelasidi, P. Liljebäck, K. Y. Pettersen, J. T. Gravdahl, Innovation in underwater robots: Biologically inspired swimming snake robots, IEEE Robotics and Automation Magazine 23 (1) (2016) 44–62.
- [9] K. McIsaac, J. Ostrowski, A geometric approach to anguilliform locomotion: modelling of an underwater eel robot, in: Proc. International Conference on Robotics and Automation (ICRA), Vol. 4, Detroit, MI, 1999, pp. 2843–2848.
- 560 [10] K. McIsaac, J. Ostrowski, Experiments in closed-loop control for an underwater eel-like robot, in: Proc. IEEE International Conference on Robotics and Automation (ICRA), Washington DC, 2002, pp. 750–755.
- [11] C. Wilbur, W. Vorus, Y. Cao, S. Currie, Neurotechnology for biomimetic robots, chapter A Lamprey-Based Undulatory Vehicle, Bradford/MIT Press, 2002.
- 565 [12] B. Li, S. Yu, S. Ma, Y. Wang, An amphibious snake-like robot with novel gaits on ground and in water, in: Proc. IASTED International Conference Intelligent Systems and Control (ISC 2011), Calgary, AB, 2011, pp. 100–105.
- [13] C. Ye, S. Ma, B. Li, Y. Wang, Locomotion control of a novel snake-like robot, in: Proc. IEEE/RSJ International Conference on Intelligent Robots and Systems (IROS), Sendai, Japan, 2004, pp. 925–930.
- 570 [14] H. Yamada, S. Chigisaki, M. Mori, K. Takita, K. Ogami, S. Hirose, Development of amphibious snake-like robot ACM-R5, in: Proc. 36th International Symposium on Robotics, Tokyo, Japan, 2005.
- [15] T. Takayama, S. Hirose, Amphibious 3d active cord mechanism "helix" with helical swimming motion, in: Proc. IEEE/RSJ International Conference on Intelligent Robots and Systems (IROS), Vol. 1, Lausanne, Switzerland, 2002, pp. 775 – 780.
- 575 [16] P. Liljebäck, Ø. Stavdahl, K. Pettersen, J. Gravdahl, Mamba - a waterproof snake robot with tactile sensing, in: Proc. International Conference on Intelligent Robots and Systems (IROS), Chicago, IL, 2014, pp. 294–301.

- 580 [17] J. Ayers, C. Wilbur, C. Olcott, Lamprey robots, in: Proc. International Symposium on Aqua Biomechanisms, 2000.
- [18] E. Kelasidi, K. Y. Pettersen, P. Liljebck, J. T. Gravdahl, Locomotion efficiency of underwater snake robots with thrusters, in: Proc. IEEE International Symposium on Safety, Security, and Rescue Robotics (SSRR), Lausanne, Switzerland, 2016, pp. 174–181.
- 585 [19] T. Knutsen, J. Ostrowski, K. McIsaac, Designing an underwater eel-like robot and developing anguilliform locomotion control, NSF Summer Undergraduate Fellowship in Sensor Technologies, Tamara Harvard University (2004) 119–142.
- [20] E. Kelasidi, K. Y. Pettersen, A. M. Kohl, J. T. Gravdahl, An experimental investigation of path following for an underwater snake robot with a caudal fin, IFAC-PapersOnLine 50 (1) (2017) 11182 – 11190, 20th IFAC World Congress.
- 590 [21] E. Kelasidi, P. Liljebäck, K. Y. Pettersen, J. T. Gravdahl, Experimental investigation of efficient locomotion of underwater snake robots for lateral undulation and eel-like motion patterns, Robotics and Biomimetics 2 (1) (2015) 1–27.
- [22] K. McIsaac, J. Ostrowski, Motion planning for anguilliform locomotion, IEEE Transactions on Robotics and Automation 19 (4) (2003) 637–625.
- 595 [23] F. Boyer, M. Porez, W. Khalil, Macro-continuous computed torque algorithm for a three-dimensional eel-like robot, IEEE Transactions on Robotics 22 (4) (2006) 763 –775.
- [24] G. Taylor, Analysis of the swimming of long and narrow animals, Proc. Royal Society of London. Series A. Mathematical and Physical Sciences 214 (1117) (1952) 158–183.
- 600 [25] M. J. Lighthill, Large-amplitude elongated-body theory of fish locomotion, Proc. Royal Society of London. Series B. Biological Sciences 179 (1055) (1971) 125–138.
- 605 [26] A. Wiens, M. Nahon, Optimally efficient swimming in hyper-redundant mechanisms: control, design, and energy recovery, Bioinspiration & Biomimetics 7 (4) (2012) 046016.
- [27] J. Chen, W. O. Friesen, T. Iwasaki, Mechanisms underlying rhythmic locomotion: body-fluid interaction in undulatory swimming, Journal of Experimental Biology 214 (4) (2011) 561–574.
- 610 [28] E. Kelasidi, K. Y. Pettersen, J. T. Gravdahl, S. Strømsøyen, A. Sørensen, Modeling and propulsion methods of underwater snake robots, in: Proc. IEEE Conference on Control Technology and Applications, Hawaii, 2017, pp. 819–826.
- [29] P. Liljebäck, K. Y. Pettersen, Ø. Stavadahl, J. T. Gravdahl, Snake Robots: Modelling, Mechatronics, and Control, Springer-Verlag, Advances in Industrial Control, 2013.
- 615

- [30] Cm labs webpage (2018).
URL <https://www.cm-labs.com/>
- 620 [31] Marine cybernetics laboratory (MC-lab) (2018). [link].
URL <http://www.ntnu.no/imt/lab/cybernetics>
- [32] Qualisys–Motion Capture Systems (2018). [link].
URL <http://www.qualisys.com>
- [33] E. Kelasidi, M. Jesmani, K. Y. Pettersen, J. T. Gravdahl, Locomotion efficiency
625 optimization of biologically inspired snake robots, *Applied Sciences* 8 (1) (2018)
80.
- [34] E. Kelasidi, K. Y. Pettersen, P. Liljebäck, J. T. Gravdahl, Integral line-of-sight for
path-following of underwater snake robots, in: *Proc. IEEE Multi-Conference on
Systems and Control*, Antibes, France, 2014, pp. 1078 – 1085.
- 630 [35] J. Guo, A waypoint-tracking controller for a biomimetic autonomous underwater
vehicle, *Ocean Engineering* 33 (17-18) (2006) 2369 – 2380.
- [36] L. Lapierre, B. Jouvencel, Path following control for an eel-like robot, in: *Proc.
MTS/IEEE International Conference Oceans*, Brest, France, 2005, pp. 460–465.
- [37] E. Kelasidi, P. Liljebäck, K. Y. Pettersen, J. T. Gravdahl, Integral line-of-sight
635 guidance for path following control of underwater snake robots: Theory and ex-
periments, *IEEE Transactions on Robotics* 33 (3) (2017) 610–628.
- [38] M. Alamir, M. El Rafei, G. Hafidi, N. Marchand, M. Porez, F. Boyer, Feedback
design for 3D movement of an eel-like robot, in: *Proc. IEEE International Con-
ference on Robotics and Automation (ICRA)*, Roma, 2007, pp. 256–261.
- 640 [39] T. I. Fossen, *Handbook of Marine Craft Hydrodynamics and Motion Control*,
John Wiley & Sons, Ltd, 2011.
- [40] E. Kelasidi, K. Y. Pettersen, J. T. Gravdahl, P. Liljebäck, Modeling of underwater
snake robots, in: *Proc. IEEE International Conference on Robotics and Automa-
tion (ICRA)*, Hong Kong, China, 2014, pp. 4540–4547.
- 645 [41] E. Kelasidi, K. Y. Pettersen, J. T. Gravdahl, Energy efficiency of underwater snake
robot locomotion, in: *Proc. 23th Mediterranean Conference on Control Automa-
tion (MED)*, Torremolinos, Spain, 2015, pp. 1124–1131.